W. WALDHAUSER*, J. M. LACKNER*#, M. KOT**, B. MAJOR***

DRY AND RINGER SOLUTION LUBRICATED TRIBOLOGY OF THIN OSSEOCONDUCTIVE METAL OXIDES AND DIAMOND-LIKE CARBON FILMS

TRIBOLOGIA SUCHYCH I SMAROWANYCH ROZTWOREM RINGERA CIENKICH FILMÓW NA BAZIE TLENKÓW METALI I DIAMENTOPODOBNYCH PROMUJĄCYCH PROCESY OSTOINTEGRACYJNE

Achieving fast and strong adhesion to jawbone is essential for dental implants. Thin deposited films may improve osseointegration, but they are prone to cohesive and adhesive fracture due to high stresses while screwing the implant into the bone, leading to bared, less osteoconductive substrate surfaces and nano- and micro-particles in the bone. Aim of this work is the investigation of the cohesion and adhesion failure stresses of osteoconductive tantalum, titanium, silicon, zirconium and aluminium oxide and diamond-like carbon films. The tribological behaviour under dry and lubricated conditions (Ringer solution) reveals best results for diamond-like carbon, while cohesion and adhesion of zirconium oxide films is highest.

Keywords: biotribology, thin films, lubrication

Osiągnięcie szybkiego i trwałego przylegania powierzchni biomateriału do kości szczęki ma zasadnicze znaczenie dla implantów dentystycznych. Cienkie osadzone filmy mogą poprawić osteointegrację ale są podatne na kohezyjne i adhezyjne pękanie podczas wkręcania implantu do kości, prowadząc do odsłoniecia mniej osteokonduktywnych powierzchni podłoża oraz powodując tworzenie się nano- i mikro cząstek. Celem niniejszej pracy są badania naprężeń wywołujących defekty w osteointegracyjnych filmach na bazie tantalu, tytanu, cyrkonu oraz tlenku aluminium i diamentopodobnych. Tribologiczne najlepsze właściwości w warunkach suchych i smarowania (roztwór Ringera) wykazały powłoki diamentopodobne, natomiast spójność i przyczepność filmy z tlenku cyrkonu.

1. Introduction

Key demand for dental screw implants is strong anchoring in jawbone. Reasonably, the thread is adapted for well-defined load transfer to bone and for preventing stress shielding from the bone. The chemistry and topography / roughness of the thread surface must provide high osteoconductivity for bone formation by osteoinduction: Osteoprogenitor cells must be stimulated to differentiate into osteoblasts for the start of new bone formation along the interface of bone and implant. However, the processes and influences on osteoinduction are scarcely understood yet. Barradas et al. stated in their review paper, that bone morphogenetic proteins are surely involved in osteoinduction, but the ability of a material to form a biological apatite layer on its surface either by dissolution / reprecipitation or by nucleation from biological fluids, is mandatory too [1]. An overview on different implant materials shows quite low osteoinductive tendency for pure metals like titanium, zirconium and tantalum as well as for widely used titanium alloys (TiAl6V4) [2-5], while chemical treatments to achieve thick oxide films, the deposition of calcium phosphate (hydroxyapatite, tricalcium phosphate, calcium phosphate, etc.) and alumina films on titanium surfaces improve bone formation and mineralization of subsequently formed extracellular matrix [1,6,7]. Similar behaviour was found for diamond-like carbon (DLC) and carbonitride films on titanium by several authors (e.g. [8-10]).

Besides optimal biocompatibility, which was tested for a wide range of inorganic thin films by the authors [11], the

*   JOANNEUM RESEARCH FORSCHUNGSGES.M.B.H., INSTITUTE FOR SURFACE TECHNOLOGIES AND PHOTONICS, FUNCTIONAL SURFACES, LEOBNER STRASSE 94, A-8712 NIKLASDORF, AUSTRIA

**   AGH UNIVERSITY OF SCIENCE AND TECHNOLOGY, FACULTY OF MECHANICAL ENGINEERING AND ROBOTICS, LABORATORY OF TRIBOLOGY AND SURFACE ENGINEERING, AL. A. MICKIEWICZA 30, 30-059 KRAKOW, POLAND,

*** POLISH ACADEMY OF SCIENCES, INSTITUTE OF METALLURGY AND MATERIALS SCIENCES 25, REYMONTA STR., 30-059 KRAKOW, POLAND

\#   Corresponding author: Juergen.Lackner@joanneum.at

application of such thin film materials on dental screw threads requires sufficient tribological properties. By cutting the thread into the bone, high shear stresses occur on the implant surface. Reasonably, the resistance of the thin film against cracking and subsequent delamination during screwing is critical. Such mechanical failure of the coating exposes at least partially the less osteoconductive substrate and leaves delaminated non-bioresorbable nano- and micro-particles in the bone. Aim of the current work is the tribological study on oxide and carbon-based thin films with high osteoconductivity. Scratch testing and reciprocating pin-on-disc testing under dry and biologically lubricated conditions are applied to simulate contact situations in jawbone and the achieved results are discussed based on topography, wetting and corrosion behaviour.

2. Experimental details

2.1. Substrate materials and film deposition

All thin films were deposited on smooth silicon (100) wafers with a resistivity in the mOhm cm^{-1} range (Wacker Siltronic, Wacker Chemie AG, Burghausen, Germany). These wafers were applied due to their highly smooth surface (arithmetic roughness R_a < 1 nm) to study principle tribological mechanisms as reference materials for surface nitrided, generally rough TiAl6V4 alloys for dental implant applications.

The substrates were cleaned before film deposition in an industrial washing machine with tenside surfactant based washing agents in order to remove contaminations from the surface. Afterwards, they were mounted in the vacuum chamber (Leybold Univex 450, Leybold Vacuum, Cologne, Germany) under laminar flow conditions (comparable to clean room class 3 (DIN ISO EN 14644-1) with <1000 particles of 0.1 μm diameter per m^3) to prevent dust contamination on the substrate surfaces. After evacuating to 4×10^{-3} Pa, the pretreatment for removing oxide layers on the silicon substrates was performed with the neutralized plasma of an anode layer ion source (ALS 340, Veeco, Fort Collins, CO, USA) [12]. Afterwards, the following coatings with 150 ±5 nm thickness were deposited (chemical compositions determined by X-ray photoelectron spectroscopy after ultra-high vacuum annealing at 350°C (oxide materials) to remove physically adsorbed carbon contaminations):

–   tantalum oxide (TaO$_x$, x = 3.06) from pure tantalum targets (99.99% Ta) by radio-frequency (13.56 MHz) magnetron sputtering (RF-MS) (3" sputtering sources (AJA Inc., North Scituate, MA, USA) with a Dressler Cesar power generator (now: Advanced Energy, Fort Collins, CO, US),
–   zirconium oxide (ZrO$_x$, x = 2.05) from pure zirconium targets (99.95% Zr) by RF-MS,
–   aluminum oxide (AlO$_x$, x = 1.76) from pure aluminum targets (99.95 % Al) by RF-MS,
–   silicon oxide (SiO$_x$, x = 2.14) from pure silicon wafer targets (Boron-doped, mOhm cm^{-1} resistance) by RF-MS,

–   titanium oxide (TiO$_x$, x = 2.09) from pure Grade-2 titanium targets by RF-MS,
–   DLC (tetrahedral amorphous hydrogenated carbon, ta-C:H) by plasma-activated chemical vapor deposition (PA-CVD) from the ALS plasma with ethyne (C$_2$H$_2$) precursor [13].

Sputtering of oxides occurred in a mixture of oxygen as reactive and argon as sputtering gas (Linde Gas, Stadl-Paura, Austria, gas quality: 99,999%). No interface layers were used in all film deposition processes at room temperature. High homogeneity in coating thickness and chemical composition was achieved by rotating the substrates in the chamber, which allowed the film deposition on all tested materials at the same time.

After film deposition, the coatings were stored under controlled atmosphere (relative humidity: 22%, temperature 21°C) till tribological testing.

2.2. Characterization

Tribological reciprocating ball-on-disc sliding experiments were performed with alumina balls with 6 mm diameter on a CSM MicroTribometer (CSM Instruments, Peseux, CH). 100, 200 and 500 mN force (equal to 0.23, 0.27 and 0.35 GPa Hertzian pressure, respectively) were chosen during sliding under 15 mm s^{-1} sliding speed, which is similar to conditions for screw insertion based on dental experience and finite element modelling. Dry tests occurred in air atmosphere (22°C, 55% relative humidity). Ringer solution (147 mmol l^{-1} Na$^+$, 4.0 mmol l^{-1} K$^+$, 2.3 mmol l^{-1} Ca^{2+}, 156 mmol l^{-1} Cl$^-$, pH = 7.4), a generally clinically used physiological infusion solution, was applied in lubricated tribological tests in liquid at 37 °C. 200 test cycles were chosen to simulate both the initial contact as well as the continuous sliding scenario.

Contact angle measurements were performed on a home-built system with 1 μl large distilled water droplets by the sessile drop method at 22°C and 51% relative humidity. The analysis occurred on samples after 2 weeks of aging in air atmosphere in the exsiccator to show steady-state conditions. The statistics in measurements is based on 5 independent measurements.

Roughness of the thin films was measured on a stylus profiler (Veeco Dektak 150, Veeco Inc., Santa Barbara, CA, USA) with a stylus with 2 μm tip radius in the mN force range. For calculating the arithmetic roughness (R_a) values, the average of 5 measured profiles with 3 mm length was applied.

Scratch testing occurred by a CSM MicroScratchTester (CSM Instruments, Peseux, CH) with a Rockwell HRC diamond cone with 0.2 mm tip radius. The scratch load was linearly increased from 0.03 to 30 N within 5 mm sliding distance. Critical loads for cohesion and adhesion cracks were defined by acoustic emission, friction force and optical inspection and given as an average value of 3 measurements.

3. Results and Discussion

A rather similar behaviour is found for all thin films on silicon for the first 200 contact cycles of sliding. This is shown for TiO$_x$ in Fig. 1: Under dry sliding conditions, generally low coefficients of friction (COF) are measured for all contact cycles, while under lubricated conditions, the initially low friction rises after several sliding cycles to higher steady-state values. The behaviour is tabled in Table 1 in dependency on the applied test load and for dry and lubricated conditions. The applied statistical values are exemplary shown in (Fig. 1): The "initial COF" gives the measured value during the first contact between the alumina ball and the coated Si. If a significant rise of the COF from the initial to a steady-state level occurs, the cycle number at the start of this behaviour is given in the column "rising friction at cycle no.". The "steady-state COF" gives the value for regime after the rise of friction. Generally, the "COF after 200 sliding cycles" is on the same level, but also a slight increase may occur. "Failure by wear" describes the visibility of wear damage by optical microscopy methods.

Under dry conditions, only TaO$_x$ films show a tribological behaviour with a step-like transition to slightly higher COF ($\Delta\mu \sim 0.10$), while all investigated film types pass the 200 contacts with either constant or slowly rising steady-state COF
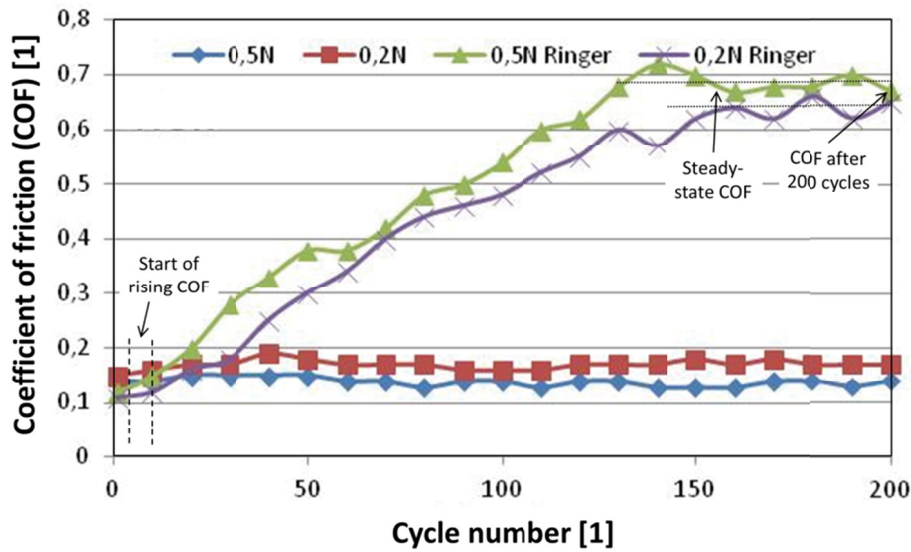

Fig. 1. Dependency of the coefficient of friction (COF) on the cycle number and normal force for sliding of an alumina ball under dry ("0.2 N" and "0.5 N") and liquid conditions (Ringer solution, "0.2 N Ringer" and "0.5 N Ringer"). Explanations for statistical values, used in (Table 1), are given

TABLE 1

Tribological properties of investigated film materials on Si under dry and Ringer solution lubricated conditions in dependency on the applied load and Hertzian pressure in the reciprocating sliding contact to a 6 mm alumina ball. The initial COF is the measured COF during the first contact, the given value after 200 cycles at the end of the experiment. In several cases, the friction coefficient rises significantly (as visible for sliding on TiO$_x$ in Ringer solution in (Fig. 1)), for which the cycle number is given. "Failure by wear" denotes the result of the optical inspection after 200 cycles testing. Full exposure of the Si substrate is labelled by "Yes", light and partial exposure by "Start". Given COFs are average values with standard deviation below 6%

| Film material	Test load (N); Hertzian pressure during test [MPa]	Dry sliding (air)					Sliding in Ringer solution				
		Initial COF [1]	Rising friction at cycle no.	Steady-state COF [1]	COF after 200 cycles [1]	Failure by wear	Initial COF [1]	Rising friction at cycle no.	Steady-state COF [1]	COF after 200 cycles [1]	Failure by wear
TaO$_x$	0.2; 271	0.12	30	0.20	0.24	Yes	0.09	2	0.60	0.59	Yes
	0.5; 352	0.08	5	0.22	0.26	Yes	0.08	2	0.48	0.48	Yes
ZrO$_x$	0.2; 271	0.14	–	0.16	0.18	Start	0.20	10	0.72	0.73	Yes
	0.5; 352	0.17	–	0.17	0.18	Yes	0.26	30	0.70	0.72	Yes
AlO$_x$	0.2; 271	0.12	–	0.17	0.19	Start	0.10	60	0.60	0.58	Yes
	0.5; 352	0.10	–	0.18	0.20	Yes	0.14	10	0.59	0.60	Yes
SiO$_x$	0.2; 271	0.09	–	0.10	0.10	No	0.12	2	0.61	0.64	Start
	0.5; 352	0.09	–	0.09	0.10	No	0.10	2	0.63	0.60	Yes
TiO$_x$	0.2; 271	0.15	–	0.16	0.17	No	0.11	10	0.65	0.66	No
	0.5; 352	0.14	–	0.14	0.14	No	0.12	2	0.69	0.67	Start
a-C:H	0.2; 271	0.06	–	0.08	0.09	No	0.08	5	0.15	0.17	No
	0.5; 352	0.07	–	0.10	0.13	No	0.06	5	0.14	0.15	No
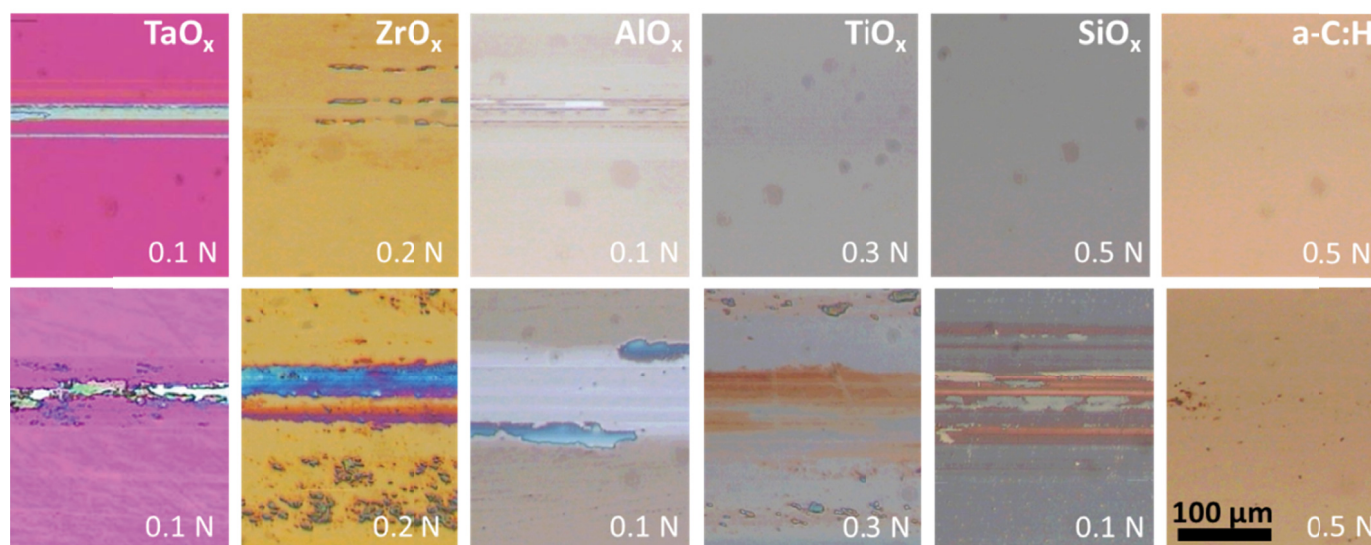
Fig. 2. Light microscopy images of the surfaces after 200 sliding cylces for sliding of an alumina ball under (upper row) dry and (lower row) (Ringer solution lubricated conditions. Chosen pictures show the lowest applied test load, for which wear was found. For TiO$_x$, SiO$_x$, and a-C:H, no wear was found at the highest applied load of 0.5 N, for which the images are shown

between 0.08-0.18. Film failure by delamination occurs for TaO$_x$ even at 0.2 N, while ZrO$_x$ and AlO$_x$ films present at such low load only first traces of wear. Nevetheless, 0.5 N force results in their total failure. This is shown in (Fig. 2) (upper row) for the central zones of the wear tracks from the reciprocating sliding experiments. Horizontal lines (or even broken lines) indicate film damage by deep scratching of the sliding ball or wear debris. Jagged framed areas are sites with full film delamination. The presented images were chosen at the lowest loads, for which wear is found. If no wear was found for SiO$_x$, TiO$_x$ and AlO$_x$ even at 0.5 N normal load, the microscopy images of sliding tracks for 0.5 N were added.

The application of the Ringer solution is used as a general test liquid in biotribology to simulate lubrication under physiological conditions. However, the introduction of the salt solution in the sliding experiments significantly rises the COF step-like ($\Delta\mu > 0.4$) after a very short run-in phase with low COF < 0.2, which lasts only 2-10 contact cycles (except for AlO$_x$ and for a-C:H films). Steady-state COF between 0.48 and 0.72 are generally found for all oxides. In contrast, the a-C:H film persists on low-friction behaviour with COF of ~0.15. Similar to dry conditions, the impact of the normal load (and, consequently, the Hertzian pressure) on the COF is negligible, while wear is dominated by tensile stresses in the films behind and shear stresses at the interface below the sliding ball. TaO$_x$, ZrO$_x$, AlO$_x$, and SiO$_x$ films delaminate from the Si substrate in the wear track even under 0.1 N normal load, while TiO$_x$ shows higher resistance (Fig. 2, lower row). No wear is found for the a-C:H film even at 0.5 N. The optical micrographs of the worn surfaces show a further feature: Interference colours in the whole sliding contact zone indicate the formation of a thin tribolayer for all oxide materials, which is missing for the dry contact situation. Energy dispersive spectroscopy analysis during scanning electron microscopy imaging revealed a high salt ion concentration

(Na, K, Ca, Cl) in these areas for the oxide materials, which is rather missing for a-C:H.

The explanation of this wear phenomena between dry and wet conditions needs the knowledge of the basic contact situations and the material-based influences like surface roughness, wetting, toughness, adhesion, (tribo-)corrosion: The lubrication effect in the Ringer solution, which has low-viscosity and is water-like, is very small: COFs drop only slightly by $\Delta\mu < 0.03$ or even increase (like for ZrO$_x$ and SiO$_x$ films) compared to dry sliding conditions. Thus, the initial contact is similar to boundary lubrication conditions, for which the viscosity of the fluid is too low to build up sufficient pressure for separating the opposed sliding surfaces [14]. Compared to dry sliding, the effect of the lubricant (water molecules) is small in boundary lubrication, because it physically adsorbs as a rather monomolecular layer on the surface and is loosely bond by van-der Waal's forces. Similar to dry conditions, asperities of the alumina ball and the coating are in contact and local sliding temperatures between 1000 and 2000°C may occur. Such high temperatures trigger the formation (deposition) of a thin salt layer from the ion-rich Ringer solution in the tribological contact zone, which is well visible in the interference contrast. Sliding on this salt film results in the high COFs, which are on rather similar level both for failed and non-failed coatings (TiO$_x$). Only the non-oxide a-C:H film is free of any visible thick salt film. The contact angle to distilled H$_2$O as model test liquid seems to have no influence on this behaviour, because the measured values for a-C:H are close to the average value of all rather hydrophobic films (Table 2).

Higher influence on salt layer formation can be expected by the surface roughness: If high asperities are contacting during the boundary lubrication conditions, the roughness has high influence on the total contact area, and the film toughness is responsible for asperity fracture [15]. Furthermore, tribolayers like the salt layer can adhere much better between the asperi-

Important properties of the investigated films relevant to the tribological behaviour: Critical loads in scratch testing
(L_{c1} for cohesive and L_{c2} for adhesive fracture), contact angle to distilled water, arithmetic roughness R_a,
and density of defects (minimum size: 0.5 µm) evaluated by light microscopy

	Critical load in scratch test [N]		Contact angle H$_2$O [°]	Roughness R_a [nm]	Approximate defect density [mm^{-2}]
	L_{c1}	L_{c2}			
TaO$_x$	14	17	78	13	1500
ZrO$_x$		22	81	18	980
AlO$_x$	19	19	108	15	570
SiO$_x$	15	19	64	22	860
TiO$_x$	14	18	76	16	350
a-C:H	12	20	90	10	790
Si substrate	22		62	2	

ties. Results of roughness measurements in (Table 2) reveal, that the arithmetic roughness R_a is small for the a-C:H films compared to all oxide films, however much higher than for the smooth polished Si substrates. The critical load L_{c1} (Table 2), defined by the first formation of cohesive cracks in the track in scratching under constantly rising load, is a measure for the film toughness and, thus, the tendency to asperity fracture. Highest toughness is evident for ZrO$_x$ films (Fig. 3), which does not show any cohesive film failure until the silicon substrate

Fig. 3. Optical micrographs of scratch tracks of selected films on silicon substrates: (a) TaO$_x$, (b) ZrO$_x$, (c) a-C:H. The left image in each row shows the surface at L$_{c1}$ for cohesive film failure with through-film cracks, the right image the surface at L$_{c2}$ for adhesive film failure with delaminations. For ZrO$_x$, no L$_{c1}$ was observed

fails at ~22 N normal load by cohesive fracture. a-C:H, TaO$_x$, TiO$_x$ and SiO$_x$ films tend to crack even at 55-70% of this load. A delamination from the silicon substrate surface in the scratch track at L_{c2}, giving hints on the film adhesion strength, is found at rather similar load for oxide films and a-C:H (lowest values for TaO$_x$ and TiO$_x$).

If asperities crack at too high stresses, wear debris forms, but is generally trapped in the contact and grinds (or ploughs) in the wear track in the subsequent sliding cycles. For boundary lubricated conditions, the occurring phenomena are extensively described by [16]. Trapped wear debris as third body rises the COF, as found e.g. for dry sliding of TaO$_x$. The higher the COF, the higher the shear forces and, thus, the stresses at the interface are [18]. Consequently, high friction due to the formed salt layer in the contact zone triggers interface failure at lower cycles, as generally found for the investigated oxide film materials.

Finally, corrosion may slightly contribute to the tribological behaviour too: Before testing, the coated silicon wafers were mounted on the tribometer and kept about 1 hour in the 37°C warm Ringer solution. Based on the very few reports on the corrosion behaviour of silicon [18,19], crevice and pitting corrosion are major mechanisms. The tested thin film materials have defect densities of 350 – 1500 mm^{-2} (Table 2), whereby the diameter of these micro-defects (mainly particles and droplets from sputtering) is in or below the micrometer range. Background for this consideration is the relatively low cohesion and adhesion of TiO$_x$ and TaO$_x$ films, which behave very different in tribological testing in Ringer solution: TaO$_x$ with high defect density wears much earlier than TiO$_x$. Furthermore, also scratching and delamination can trigger (tribo-)corrosion, however mainly for higher tribological contact cycle numbers than tested in this work.

4. Conclusions

In conclusion, we found two different types of tribological behaviour for oxide thin film materials and a-C:H: Oxide materials show early failure under dry and, especially, Ringer solution lubricated tribological conditions, whereby the cohesion strength
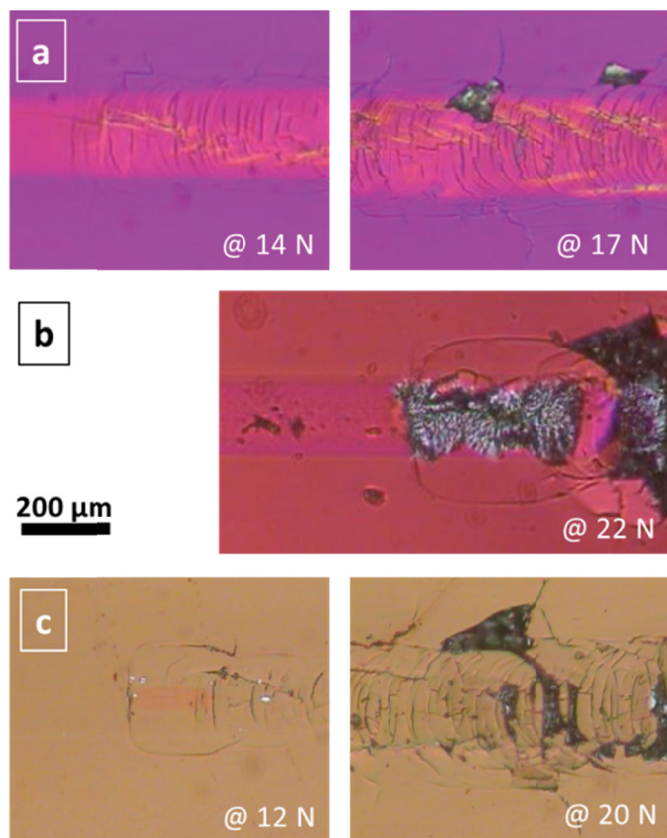
of the thin films is decisive for long lifetime without wear. In contrast, the smoother a-C:H film possess an anti-adhesive, low-friction behaviour both under dry and Ringer solution conditions, although the cohesion and adhesion strength is only low compared to the oxides. No salt deposit is formed in the wear track of a-C:H in contrast to the oxides, which seems to cause high friction coefficients and their tribological failure.

Based on these initial results on highly smooth silicon substrates, further studies will be focused on rougher substrates (nitrided TiAl6V), the detailed analysis of the salt layer formation mechanisms and will additionally include proteins and cortical bone as counterbody for a best approach to mechanisms in the body.

REFERENCES

[1] A.M.C. Barradas, H. Yuan, C.A. van Blitterswijk1, P. Habibovic, Europ Cells Mater **21**, 407 (2011).

[2] J.D. de Bruijn, H. Yuan, R. Dekker, P. Layrolle, K. de Groot, C.A. van Blitterswijk, in: J.E. Davies (ed.), Bone Engineering, Toronto, Canada, 421 (2000).

[3] F. Barrere, C.M. van der Valk, R.A. Dalmeijer, G. Meijer, C.A. van Blitterswijk, K. de Groot, P. Layrolle, J Biomed Mater Res **66A**, 779 (2003).

[4] P. Habibovic, T.M. Sees, M.A. van den Doel, C.A. van Blitterswijk, K. de Groot, J Biomed Mater Res A **77**, 747 (2006).

[5] J. Li, P. Habibovic, H. Yuan H, M. van den Doel, C.E. Wilson, J.R. de Wijn, C.A. van Blitterswijk, K. de Groot, Biomaterials **28**, 4209 (2007).

[6] S. Fujibayashi, M. Neo, H.M. Kim, T. Kokubo, T. Nakamura, Biomaterials **25**, 443 (2004).

[7] H. Yuan, J.D. de Bruijn, X. Zhang, C.A. van Blitterswijk, K. de Groot K, in: Proc Eur Conf Biomater, London, UK, 209 (2001).

[8] A.P. Rubstein, E.B. Makarova, I.S. Trakhtenberg, I.P. Kudryavtseva, D.G. Bliznets, Y.I. Philippov, I.L. Shlykov, Diam Relat Mater **22**, 128 (2012).

[9] R. Olivares, S.E. Rodil, H. Arzate, Diam Relat Mater **16**, 1858 (2007).

[10] F.Z. Cui, X.L. Qing, D.J. Li, J. Zhao, Surf Coat Technol **200**, 1009 (2005).

[11] J.M. Lackner, W. Waldhauser, Coatings; submitted (2015).

[12] J.M. Lackner, W. Waldhauser, M. Schwarz, L. Mahoney, L. Major, B. Major, Vacuum **83**, 302 (2008).

[13] J.M. Lackner, W. Waldhauser W. AIP Proc., submitted (2015).

[14] D. Godfrey, NASA **SP-181**, 335 (1968).

[15] K. Holmberg, A. Matthews, Coatings tribology, Amsterdam, Elsevier (1994).

[16] K. Komvopoulos, N.P. Suh, N. Saka, Wear **107**, 107 (1968).

[17] J.M. Lackner, W. Waldhauser, L. Major, M. Kot, Coatings **4**, 121 (2014).

[18] D.D. Zhou, R.J. Greenberg, in: D.D. Zhou, E. Greenbaum (eds.). Implantable Neural Prostheses 1, Biological and Medical Physics, Biomedical Engineering, Berlin, Springer Science Business Media, 1 (2009).

[19] D. Zhou, B. Mech, R. Greenberg, Proc 198th Electrochem Soc Meet, 363 (2000).